Non–isothermal two–phase hydrogen transport in rock salt during cycling in underground caverns

Murad S. Abuaisha, Ahmed Rouabhi, Joel Billiotte, Faouzi Hadj-Hassen

Non–isothermal two–phase hydrogen transport in rock salt during cycling in underground caverns

Murad AbuAisha[a,*], Ahmed Rouabhi[a], Joël Billiotte[a], Faouzi Hadj–Hassen[a]

[a] *MINES ParisTech, PSL Research University, Centre de Géosciences, 35 rue Saint Honoré, 77300, Fontainebleau, France*

Abstract

For a good management and precise tracks of hydrogen quantities stored in salt caverns, this paper presents a study on hydrogen transport in rock salt during cycling. It provides a novel mathematical–numerical model that couples the cavern thermodynamics with the transport mechanisms of hydrogen in the saturated rock salt in a fully coupled thermo–hydraulic framework. Both the two–phase Darcian percolation and the Fickian diffusion are used to account for hydrogen migration in the interstitial brine of the rock salt. Due to the absence of experimental data, a parametric study is furnished. The effect of cycling within the cavern on the migration mechanisms is discussed in detail. Simulations have confirmed the dependency of the Darcian percolation on the model parameters. However, for similar applications, this dependency might be limited. The value of the Fickian diffusion coefficient affects indirectly the Darcian percolation. The two–phase percolation becomes more of a piston–like for very small values of the diffusion coefficient. On a real–scale typical cavern, and over a period of 40 years, simulations have proven that the quantity of hydrogen lost into the surrounding rock salt is unimportant. Besides, cycling renders this quantity more insignificant.

Keywords: Underground salt caverns; hydrogen transport; cavern thermodynamic state; hydrogen percolation and diffusion; two–phase flow, Fickian diffusion; thermo–hydraulic coupling

1. Introduction

Driven by concerns related to climate change, energy transition has led to the use of new clean energy resources [1]. Hydrogen has been regarded as an important energy vector in this transition [2–4]. However, the increasing energy demands and the intermittency problems [5–7] require large–scale storage techniques [8, 9]. Underground salt caverns offer the most promising option owing to their low investment cost and low cushion gas requirement [9]. Rock salt/halite occurs within sedimentary rocks where it has formed from the evaporation of seawater or salty lakes. Rock salt is consequently deposited in cycles

*Corresponding author
Email addresses: murad.abuaisha@mines-paristech.fr (Murad AbuAisha), ahmed.rouabhi@mines-paristech.fr (Ahmed Rouabhi), joel.billiotte@mines-paristech.fr (Joël Billiotte), faouzi.hadj_hassen@mines-paristech.fr (Faouzi Hadj–Hassen)

which affects its directional properties like the elastic modulus and the permeability. Depending on the location, the rock salt properties, mechanical and hydraulic, differ as well.

During cavern operation, hydrogen undergoes changes in its temperature and pressure. Such changes are expected to affect its migration into the surrounding rock domain. Hydrogen invasion into this embracing rock takes place either through the rock salt itself, or through the more permeable and porous interlayers (if they happen to exit). Since underground storage caverns are constructed in networks, the lost hydrogen into the surrounding rock can weaken the neighboring caverns structure. Moreover, the cost of hydrogen production as well as a good management of storage require to keep precise tracks of the injected and withdrawn hydrogen quantities. Studies addressing hydrogen or gas transport through rock salt are scarce. For instance, *Liu et al.* [10] provided a cavern scale study to estimate the hydrogen tightness. Their approach assumed that hydrogen filtrates through the rock salt following a Darcian flow type. Besides, they assigned a relatively small permeability value to the rock salt while assuming a zone of dilatancy. They eventually concluded that the salt caverns are hydrogen–tight except for the regions of interlayers which can also be considered as hydrogen–tight for permeabilities less than 10^{-18} m^2. *Liu et al.* [11] presented a general study about gas tightness of abandoned salt caverns. Though their study did not include hydrogen, they have concluded that the permeability of the interlayers was a key factor in influencing gas seepage in the vicinity of the caverns and that interlayers formed primary channels for gas migration. They used as well a generalized Darcian flow type model to evaluate the fluid seepage around the cavern. They found that the upper threshold permeability of the interlayers must be no more than 10^{-16} to 10^{-17} m^2 to guarantee tightness when storing natural gas, and no more than 10^{-16} m^2 when storing oil. There are, however, considerable research papers that treat hydrogen percolation and diffusion in the clay sedimentary basins in the context of radioactive waste storage [12, 13].

Since rock salt contains interstitial brine and characterized by extremely low permeabilities and porosities, the application of one–phase generalized Darcian flow to describe hydrogen transport is questioned. Moreover, none of the available literature is addressing the effect of cavern cycling on the migration mechanisms. Indeed, the cavern thermodynamic state is a function of cycling. Consequently, in the cavern vicinity, both the interstitial rock salt brine pressure and temperature evolutions are functions of cycling as well. These changes in the interstitial brine pressure and temperature must influence the migration of hydrogen into the rock domain. The novelty of this research stems from providing a mathematical–numerical model that couples the cavern thermodynamics with the non–isothermal transport mechanisms of hydrogen into the rock salt. Both the Darcian two–phase percolation and the Fickian diffusion are considered as well as the interaction between them. This model addresses as much as possible of the problem complex physics for good estimation of the exchanged hydrogen mass. Besides, it precisely presents effect of cycling. Due to the absence of any literature or experimental data treating hydrogen migration in saturated rock salt, we offered a parametric study that investigated the effect of the two–

phase van Genuchten model parameters as well as the Fickian diffusion coefficient on the total mass of exchanged hydrogen. The van Genuchten model allows to describe the two–phase percolation of hydrogen (characterized by very low viscosity) in rock salt (characterized by very small pore size)[1]. Eventually, an overestimating scenario of model parameters, of diffusion coefficient, and of boundary conditions, was considered to estimate the amount of hydrogen migrated during a 40–year period of hydrogen cycling in a typical spherical cavern.

This paper proceeds as follows: the problem of hydrogen migration in the context of underground storage is first presented; the expected transport mechanisms between the cavern phases are discussed; the mathematical and numerical models are then shown for cycling in a typical spherical cavern; after the parametric study is implemented, an overestimating scenario is simulated for a 40–year time period of cycling. The simulations have shown that even for a pessimistic scenario of overestimating model parameters and boundary conditions, the amount of lost hydrogen into the rock domain rests very negligible compared to the cycled mass of hydrogen.

2. Hydrogen migration in rock salt

This section aims at addressing the problem of hydrogen exchange/transport mechanisms in the context of underground storage. Each mechanism is described briefly and an overall conclusion is eventually drawn about the mechanism that will be considered in the simulations.

2.1. Hydrogen storage in salt caverns

Solution mining is commonly used to create large caverns in rock salt formations. In this process, a single well, drilled from the ground surface to the targeted depth (Fig. 1(a)), is generally used to inject fresh water and withdraw brine through a concentric tubing system (the leaching process) [16, 17]. Once leaching is completed, brine within the cavern is reduced to minimal quantities by a debrining/filling phase where it is moved out by hydrogen injection [18, 19].

Figure 1(a) shows an underground cavern filled with hydrogen at a certain pressure and temperature. The figure also depicts the amount of brine left in the cavern at the end of the debrining process. Hydrogen within the cavern is expected to experience cycles of pressure and temperature changes according to the intended usage. During its life time, the cavern mainly contains, simultaneously or sequentially, two different immiscible phases: the stored hydrogen and the brine. The third important phase of this storage outline is the surrounding rock salt domain. This domain is constituted of the salt mass which itself is a mixture of grains or crystals of halite and the brine occupying the inter–grain spaces. Each of the

[1]This type of percolation is defined using the capillary and mobility numbers, for details see *Yortsos et al.* [14], *Lenormand* [15]

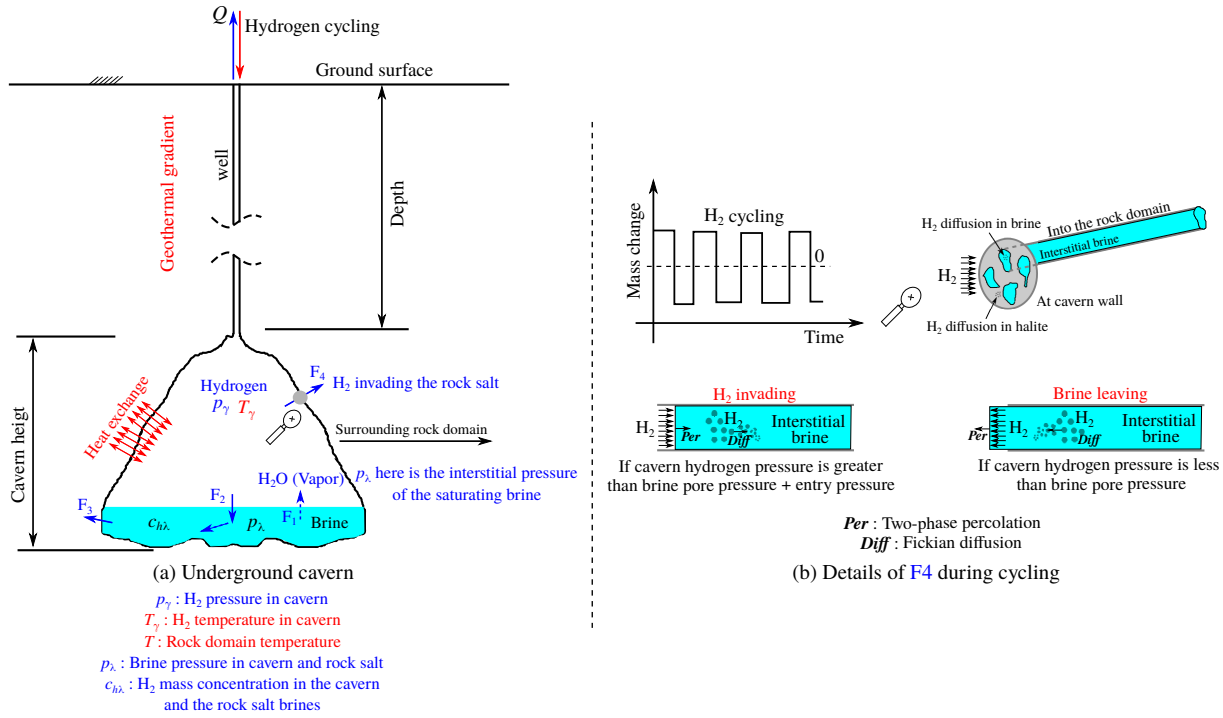

Figure 1: (a) Schematic representation of hydrogen storage in salt caverns and its transport mechanisms between phases. (b) Transport of hydrogen into the rock salt domain (flux F_4).

three phases is characterized by state variables which are for hydrogen: the pressure and the temperature, for brine: the pressure, the temperature, the salt concentration, and the hydrogen concentration, for the rock salt: the stress and the temperature. Since hydrogen may be present in the non–gaseous phase in the other phases (brine and solid), its presence will be characterized by a mass concentration.

While the cavern is operated, the three phases are interacting as follows (Fig. 1(a)): brine is evaporating into the stored hydrogen (F_1); hydrogen is dissolving in the brine (F_2) and is percolating and diffusing into the porous rock salt (F_4); brine at the cavern bottom is flowing into the rock salt with its dissolved hydrogen (F_3).

2.2. Transport mechanisms

Transport mechanisms between phases include three components: the cavern hydrogen–brine interaction; the brine–rock salt interaction; and the hydrogen–rock salt interaction. The first component happens at the hydrogen–brine interface within the cavern where hydrogen dissolves in brine (flow F_2 in Fig. 1(a)) according to Henry's law [20]. The dissolution induces a flow of hydrogen in the brine which enriches the hydrogen concentration by diffusion [21, 22] and convection [24, 25].

In the second component the brine–rock salt interface moves depending on the degree of salinity of the cavern brine. Salt can precipitate from brine onto the interface or the interface can be worn away

by the brine to achieve saturation continuity at the cavern working temperature and pressure [26–28]. As the cavern brine pressure is equal to the cavern hydrogen pressure, cavern brine can flow into the saturated rock salt, or the interstitial rock salt brine can move out into the cavern (flow F_3 in Fig. 1(a)). Due to the ambiguity with regard to knowing the inter–grain connectivity of rock salt, the pressure of the interstitial brine is poorly defined. However, its value can be limited to two extreme values [29]:

1. the so–called halmostatic pressure, which considers that the brine occupies a totally connected space in the rock mass. Consequently, this pressure is the equivalent to the hydrostatic pressure calculated using the brine density;
2. a lithostatic pressure, which considers that the brine occupies an isolated space in the rock salt phase. Therefore, the brine pressure is assumed in equilibrium with the geologic stresses of the rock salt mass. This pressure extremity is calculated using the rock salt density [30].

At the hydrogen–rock salt interface (see also Fig. 1(b)), the penetration of hydrogen into the saturated rock salt (flow F_4 in Fig. 1(a)) can take place either [31]:

1. in the solid phase itself, i.e. the halite crystals;
2. in the interstitial brine.

These are two different mechanisms, the first is equivalent to hydrogen diffusion in the solids [32, 33]. The second includes hydrogen Fickian diffusion in the interstitial brine and the two–phase Darcian percolation [13, 34, 35].

During cycling, the fluxes F_2, F_3, and F_4 need to be considered in order to calculate the total mass of exchanged hydrogen. Only flow F_4 will be considered in this research paper. Flows F_2 and F_3 will be addressed in a future research.

3. Mathematical and numerical models

This section presents the mathematical and numerical models needed to evaluate the quantity of hydrogen transported to the rock salt domain surrounding a typical underground cavern. Simulations are done for a seasonal cycling in a spherical cavern created at 910 m depth and for a 40–year time period.

3.1. The mathematical model

The mathematical model couples the hydrogen thermodynamics in the cavern with the non–isothermal hydrogen transport in the saturated rock salt domain. To simplify the problem, the following assumptions are made. Some assumptions are adopted for an overestimating study:

1. the underground cavern is assumed to be filled with a mono–component single–phase hydrogen;

2. hydrogen cycling is seasonal/slow, consequently, a uniform thermodynamic state is assumed within the cavern [36];
3. rock salt domain is assumed saturated with brine;
4. for an overestimating study, brine pressure within the rock salt domain is assumed halmostatic;
5. for an overestimating study, rock salt creep due to cavern operation is neglected;
6. hydrogen diffusion in the halite structure is neglected;
7. hydrogen concentration is initially disregarded in the rock salt domain;
8. rock salt, interstitial brine, and the invading hydrogen are assumed in thermal equilibrium;
9. hydrogen invasion into the rock salt domain is assumed to follow the van Genuchten percolation model [14, 15];
10. for an overestimating study, hydrogen entry pressure into the saturated rock salt is neglected.

Hydrogen thermodynamics in underground caverns is presented in the work of *Rouabhi et al.* [37] and *AbuAisha and Rouabhi* [36]. As an example to modeling a uniform thermodynamic state within the cavern, the following system of equations is used:

$$\begin{aligned} \text{mass balance:} \quad & \mathcal{M}\big(-\chi_{p\gamma}\,\dot{T}_\gamma + \chi_{T\gamma}\,\dot{p}_\gamma\big) &&= Q_e - \mathfrak{S}; \\ \text{energy balance:} \quad & \mathcal{M}\,C_{p\gamma}\,\dot{T}_\gamma - \mathcal{V}\,\chi_{p\gamma}\,T_\gamma\,\dot{p}_\gamma &&= Q_e^+\,C_{p\gamma}(T_\gamma^{\text{inj}} - T_\gamma) - \Psi, \end{aligned} \tag{1}$$

where $\mathcal{M}$ (kg) is the cavern hydrogen mass, T_γ (K) is the cavern uniform hydrogen temperature, $\chi_{p\gamma}$ (1/K) is the hydrogen isobaric thermal expansivity, p_γ (Pa) is the cavern uniform hydrogen pressure, $\chi_{T\gamma}$ (1/Pa) is the hydrogen isochoric compressibility, Q_e (kg/s) is the well/external flow rate, Q_e^+ is the positive/injection part of Q_e, $\mathfrak{S}$ (kg/s) is the internal/exchanged mass rate between the cavern and the rock domain, $C_{p\gamma}$ (J/kg/K) is the hydrogen heat capacity at a given pressure, $\mathcal{V}$ (m^3) is the cavern volume, T_γ^{inj} (K) is the injection temperature, and Ψ (W) is the power exchanged between the cavern hydrogen and the surrounding rock. Both the exchanged power Ψ and mass rate $\mathfrak{S}$ are positive when given to the rock domain.

Once the cavern thermodynamic state (p_γ and T_γ) is known, it can be used to calculate the hydrogen invasion into the surrounding rock salt domain. Figure 1(b) shows the mechanisms related to hydrogen transport in the saturated rock salt while assuming a van Genuchten two–phase percolation. When hydrogen pressure within the cavern exceeds the rock salt pore pressure plus the entry pressure, hydrogen invades the rock salt in a two phase percolation type flow. However, when hydrogen pressure becomes less than the interstitial brine pressure, brine moves towards the cavern and tends to pour down the cavern wall. Fickian diffusion of hydrogen in the rock salt interstitial brine is function of hydrogen cycling. This diffusion is related to the hydrogen mass concentration gradient between the cavern and

the rock salt domain. The temperature changes within the cavern lead to temperature changes in the rock salt domain. In this study, rock salt, interstitial brine, and the invading hydrogen are assumed to be in local thermal equilibrium. Besides, a temperature continuity is assumed at the cavern wall. The thermo-hydraulic coupling in the rock domain is accounted for through the pressure and temperature effects on the hydrogen and the brine densities.

As the mechanical deformation of the rock salt is neglected, the subsequent percolation–diffusion equations are established in the initial configuration of the solid matrix. The rock salt porosity is denoted by n, and T denotes the temperature for all the phases in the rock salt domain. For each fluid phase $\alpha \in \Big\{\lambda \text{ (liquid)}, \gamma \text{ (gas)}\Big\}$, p_α stands for the pressure, n_α the partial porosity, $S_\alpha = n_\alpha/n$ the saturation degree, and ρ_α (kg/m^3) the density. In the liquid phase λ, $c_{h\lambda}$ denotes the mass concentration of hydrogen and $\rho_{h\lambda} = c_{h\lambda}\,\rho_\lambda$ denotes its density. For a given quantity X, the apparent value (per unit volume of the entire porous medium) is denoted X^α with $X^\alpha = n_\alpha\, X_\alpha$, where X_α is per unit volume occupied by the α–phase.

The rock salt interstitial brine density is characterized by four state variables which are the brine pressure p_λ, its temperature T, the hydrogen concentration $c_{h\lambda}$, and the salt concentration. In this study, the interstitial brine is assumed saturated with salt at any time. Besides the mass of the dissolved hydrogen is assumed very minor to affect the brine density. Therefore, the mass balance equations of the components b (brine) and h (hydrogen) of the liquid phase can be written in the following form [38–40],

$$\begin{aligned}
\dot{m}_b^\lambda + \boldsymbol{\nabla}.\Big[\rho_\lambda\big(1-c_{h\lambda}\big)\boldsymbol{v}_\lambda - \rho_\lambda\,\boldsymbol{\mathcal{J}}_{h\lambda}\Big] &= \pi_b,\\
\dot{m}_h^\lambda + \dot{m}^\gamma + \boldsymbol{\nabla}.\Big[\rho_\lambda\big(c_{h\lambda}\boldsymbol{v}_\lambda + \boldsymbol{\mathcal{J}}_{h\lambda}\big) + \rho_\gamma \boldsymbol{v}_\gamma\Big] &= \pi_h,\\
\text{with}\quad m^\alpha = nS_\alpha\rho_\alpha \quad \text{for} \quad \alpha \in \{\lambda,\gamma\},&\\
m_b^\lambda = (1-c_{h\lambda})\,m^\lambda, \quad \text{and} \quad m_h^\lambda = c_{h\lambda}\,m^\lambda,&
\end{aligned} \tag{2}$$

where ρ_α is the density of the α–phase, $\boldsymbol{v}_\alpha$ (m/s) is the filtration velocity of the α–phase, $\boldsymbol{\mathcal{J}}_{h\lambda}$ (m/s) is the Fickian diffusion of hydrogen in the liquid phase λ, π_b and π_h (kg/m^3/s) are the total mass creation terms of the two components in the fluid phase. If heat convection in the rock salt domain is neglected, the following energy equation can be used to describe heat transfer within the rock salt domain due to cycling in the cavern,

$$\begin{aligned}
m\,C_p\,\dot{T} + \boldsymbol{\nabla}.\boldsymbol{\psi} = 0,&\\
\text{with,}\quad m\,C_p = \sum_\alpha m^\alpha C_{p\alpha}, \quad \text{and,} \quad \boldsymbol{\psi} = -\underline{\underline{\boldsymbol{\Lambda}}}.\boldsymbol{\nabla}T,&
\end{aligned} \tag{3}$$

with $\alpha \in \{\lambda,\, \gamma,\, \sigma \text{ (solid)}\}$, and $\underline{\underline{\boldsymbol{\Lambda}}}$ (W/m/K) is the saturated rock salt domain thermal conductivity tensor. If the thermal conductivities of the three phases are assumed isotropic, the domain thermal

conductivity Λ is expressed by the geometric mean of the phases thermal conductivities [41],

$$\Lambda = \Lambda_{\sigma}^{n_{\sigma}} \, \Lambda_{\lambda}^{n_{\lambda}} \, \Lambda_{\gamma}^{n_{\gamma}}. \tag{4}$$

In a two–phase percolation flow, the liquid saturation degree S_{λ} can be calculated using the *van Genuchten* [42] expression,

$$\tilde{S}_{\lambda} = \frac{S_{\lambda} - S_{\lambda r}}{S_{\lambda s} - S_{\lambda r}} = \left(1 + \left(\frac{p_c}{P_r}\right)^{1/(1-\ell)}\right)^{-\ell}, \tag{5}$$

where $p_c = p_{\gamma} - p_{\lambda}$ is the capillary pressure, $\tilde{S}_{\lambda}$ is the effective degree of saturation, the parameters $S_{\lambda r}$ and $S_{\lambda s}$ represent the liquid residual and maximum saturation values respectively ($S_{\lambda} \in [S_{\lambda r} - S_{\lambda s}]$), ℓ and P_r (Pa) are model parameters. The equation does not introduce the notion of an entry pressure as it will be neglected in this research.

The hydraulic problem (Eq. 2) needs to be completed with constitutive and state laws. The filtration velocity vectors are assumed to follow a Darcian flow nature,

$$\boldsymbol{v}_{\alpha} = -\frac{k_{r\alpha}}{\mu_{\alpha}} \underline{\underline{\boldsymbol{k}}}.(\boldsymbol{\nabla} p_{\alpha} - \rho_{\alpha} \mathbf{g}), \quad \text{for} \quad \alpha \in \{\lambda, \gamma\}, \tag{6}$$

where $\underline{\underline{\boldsymbol{k}}}$ (m^2) is the intrinsic permeability tensor, μ_{α} (Pa s) is the dynamic viscosity of the α–phase, $\mathbf{g}$ ($\mathrm{m/s}^2$) is the gravitational acceleration vector, and $k_{r\alpha}$ is the relative permeability of the α–phase. Relative permeabilities can be calculated using the Mualem–van Genuchten model [43],

$$k_{r\lambda} = \sqrt{\tilde{S}_{\lambda}} \left[1 - \left(1 - \tilde{S}_{\lambda}^{1/\ell}\right)^{\ell}\right]^2, \quad \text{and} \quad k_{r\gamma} = \sqrt{1 - \tilde{S}_{\lambda}} \left(1 - \tilde{S}_{\lambda}^{1/\ell}\right)^{2\ell}. \tag{7}$$

The diffusion vector of hydrogen in the liquid phase is related to the concentration gradient through the Fick's law,

$$\boldsymbol{\mathcal{J}}_{h\lambda} = -\underline{\underline{\boldsymbol{D}}}_{h\lambda}.\boldsymbol{\nabla} c_{h\lambda} = c_{h\lambda}(\boldsymbol{v}_{h\lambda} - \boldsymbol{v}_{\lambda}), \tag{8}$$

where $\underline{\underline{\boldsymbol{D}}}_{h\lambda}$ (m^2/s) and $\boldsymbol{v}_{h\lambda}$ (m/s) are the diffusivity coefficient tensor and the diffusive velocity of hydrogen in the λ–phase respectively. This coefficient can be determined experimentally for a given component, a phase, and a porous medium [44], or empirically from the plain diffusivity in the liquid phase ($\bar{D}_{h\lambda}$) modified by the characteristics of the porous network (porosity, turtuosity, and constrictivity). A commonly used expression is $D_{h\lambda} = \bar{D}_{h\lambda} \, n^q$, where q is an empirical parameter that generally lies between 1.8 and 2.4 [21]. The exchanged hydrogen mass rate between the cavern and the surrounding rock salt can, therefore, be calculated as,

$$\mathfrak{S} = \underbrace{\int_{\mathcal{S}} \rho_{\gamma} \, \boldsymbol{v}_{\gamma}.\boldsymbol{n} \, d\mathcal{A}}_{\text{Percolated mass rate}} + \underbrace{\int_{\mathcal{S}} \rho_{\lambda} (\boldsymbol{\mathcal{J}}_{h\lambda} + c_{h\lambda} \, \boldsymbol{v}_{\lambda}).\boldsymbol{n} \, d\mathcal{A}}_{\text{Diffused mass rate}}, \tag{9}$$

with $\boldsymbol{n}$ being the outward unit vector normal to the cavern surface.

The hydrogen phase is assumed to behave as a real gas (see Appendix A). The state equation is described using the two state functions; the density $\rho_\gamma(p_\gamma, T_\gamma)$, and the heat capacity $C_{p\gamma}(T_\gamma)$ at a given pressure. The thermodynamic variables are related to each other through the formula $p_\gamma = \rho_\gamma\, T_\gamma\, Z$, with Z (J/kg/K) being the gas compressibility factor. The chemical potential equality between the λ– and γ–phases leads to the definition of the Henry's law $p_\gamma = (K_H/M_h)\rho_{h\lambda} = Hc_{h\lambda}$, with K_H (L Pa/mol) being the Henry's constant, M_h (kg/mol) the hydrogen molecular weight, and $H = K_H\,\rho_\lambda/M_h$ (Pa). The brine phase is assumed to be slightly compressible, i.e. $\dot{\rho}_\lambda/\rho_\lambda = \chi_{T\lambda}\,\dot{p}_\lambda - \chi_{p\lambda}\,\dot{T}$ with $\chi_{T\lambda}$ (1/Pa) and $\chi_{p\lambda}$ (1/K) being the isochoric compressibility and the isobaric thermal expansion coefficient respectively.

3.2. Saturated/unsaturated state transition

The set of differential equations and primary variables (Eq. 2) needs to be controlled to assure the transition from fully saturated state to unsaturated state, or vice versa. In this paper, we only consider the problem of hydrogen appearance in rock salt where the brine phase is always present. The modeling approach of *Mahjoub et al.* [39] is proposed. It consists of using the dissolution and diffusion phenomena to derive a set of differential equations applicable for both saturated and unsaturated states.

The choice of the primary variables is crucial. The pressure p_λ can be chosen as the first primary variable because the brine phase is assumed present at any time. With regard to the second unknown, due to dissolution and diffusion phenomena, the mass concentration $c_{h\lambda}$ is a permanent unknown, whether the medium is saturated or unsaturated. Thus, it is chosen as the second primary variable. However, to assure the homogeneity in the primary variables, a pseudo–hydrogen pressure is defined as $\tilde{p}_\gamma = Hc_{h\lambda}$. It represents the real hydrogen pressure only when the hydrogen phase is present ($\tilde{p}_\gamma = p_\gamma$ if $S_\lambda < 1$), and it is just a definition in the saturated case. To use the same equations in the saturated case, a new pseudo–capillary pressure is introduced $\tilde{p}_c = \tilde{p}_\gamma - p_\lambda$. The saturation degree is expressed as a function of this pseudo–capillary pressure such that $S_\lambda(\tilde{p}_c) = S_\lambda(p_c)$ when $\tilde{p}_c \geq 0$ (because $\tilde{p}_c = p_c$), and $S_\lambda(\tilde{p}_c) = 1$ when $\tilde{p}_c < 0$.

Taking these definitions into consideration, the γ–Darcy and Fick laws have to be reformulated and integrated into the conservation equations. The same equation for γ–Darcy law (Eq. 6) can be used after replacing p_γ by $\tilde{p}_\gamma$, with $\rho_\gamma(\tilde{p}_\gamma, T_\gamma)$. In Fick's law (Eq. 8), $c_{h\lambda}$ is replaced by $\tilde{p}_\gamma/H$, and the variation of H is assumed negligible compared to the variation of $\tilde{p}_\gamma$. The reformulated mass conservation equations

can be cast into the following system of coupled partial differential equations,

$$
\begin{aligned}
\dot{m}_b^\lambda - \boldsymbol{\nabla}.\Big(\underline{\underline{\boldsymbol{\mathcal{B}}}}_{b\lambda}.(\boldsymbol{\nabla} p_\lambda - \rho_\lambda \mathbf{g}) + \underline{\underline{\boldsymbol{\mathcal{B}}}}_{b\gamma}.\boldsymbol{\nabla}\tilde{p}_\gamma\Big) &= \pi_b, \\
\dot{m}_h^\lambda + \dot{m}^\gamma - \boldsymbol{\nabla}.\Big(\underline{\underline{\boldsymbol{\mathcal{B}}}}_{h\lambda}.(\boldsymbol{\nabla} p_\lambda - \rho_\lambda \mathbf{g}) + \underline{\underline{\boldsymbol{\mathcal{B}}^{\boldsymbol{f}}}}_{h\gamma}.\boldsymbol{\nabla}\tilde{p}_\gamma + \underline{\underline{\boldsymbol{\mathcal{B}}^{\boldsymbol{p}}}}_{h\gamma}.(\boldsymbol{\nabla}\tilde{p}_\gamma - \rho_\gamma \mathbf{g})\Big) &= \pi_h, \\
\text{with} \quad \underline{\underline{\boldsymbol{\mathcal{B}}}}_{b\lambda} = \big[(1-c_{h\lambda})\rho_\lambda k_{r\lambda}/\mu_\lambda\big]\underline{\underline{\boldsymbol{k}}}, \quad \underline{\underline{\boldsymbol{\mathcal{B}}}}_{b\gamma} &= (-\rho_\lambda/H)\underline{\underline{\boldsymbol{D}}}_{h\lambda}, \\
\underline{\underline{\boldsymbol{\mathcal{B}}}}_{h\lambda} = (c_{h\lambda}\rho_\lambda k_{r\lambda}/\mu_\lambda)\underline{\underline{\boldsymbol{k}}}, \quad \underline{\underline{\boldsymbol{\mathcal{B}}^{\boldsymbol{f}}}}_{h\gamma} = (\rho_\lambda/H)\underline{\underline{\boldsymbol{D}}}_{h\lambda}, \quad \text{and,} \quad \underline{\underline{\boldsymbol{\mathcal{B}}^{\boldsymbol{p}}}}_{h\gamma} &= (\rho_\gamma k_{r\gamma}/\mu_\gamma)\underline{\underline{\boldsymbol{k}}}.
\end{aligned}
\tag{10}
$$

3.3. The numerical model

The numerical model represents a spherical cavern of volume $\mathcal{V} = 300,000$ m^3 in a surrounding rock domain. The well extends from the surface at $z = 0$ m to the cavern top at $z = z_w = -910$ m (Fig. 2(a)). The cavern has been leached (full of brine) and is initially in thermal equilibrium with the surrounding rock domain at $T = 40$ °C. The brine pressure within the cavern is also in equilibrium with the rock salt pore pressure at the halmostatic value of $p_\lambda = -\rho_\lambda\, \mathrm{g}\, z = 11.2$ MPa. The cavern brine is then replaced by hydrogen during a debrining/filling phase of 90 days where hydrogen pressure of 22 MPa is attained within the cavern. The cavern is later left unsolicited for a similar period of time. Consequently, after 90 days of standstill, the cavern volume averaged temperature and pressure are 46 °C and 22 MPa respectively. Cavern then undergoes seasonal cycling following the program shown in Fig. 2(b) for a 40–year time period, where hydrogen is injected at $T_\gamma^{\mathrm{inj}} = 40$ °C

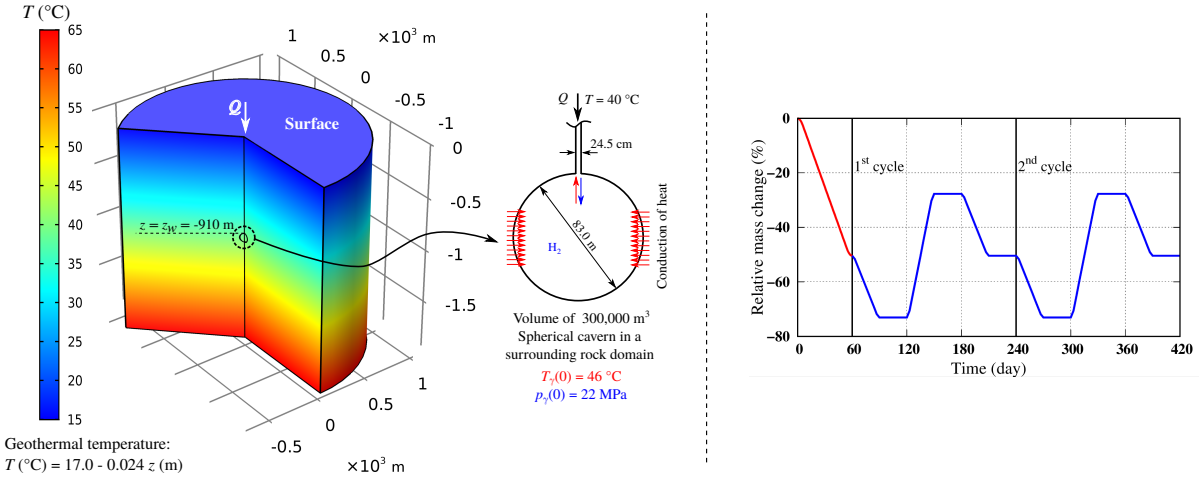

(a) Typical spherical cavern

(b) Imposed mass variations (cycling)

Figure 2: (a) Schematic diagram of the boundary value problem: it represents a spherical cavern created at 910 m depth in a surrounding rock salt domain. The cavern has been filled with hydrogen during a 90–day time period, and then left unsolicited for an equivalent period of time. This has led to a cavern volume averaged temperature and pressure of 46 °C and 22 MPa respectively. (b) Imposed cavern relative mass variations; only the first two cycles are shown.

Figure 2(b) shows the cycling scheme that will be considered in our simulations in terms of relative mass change $\tilde{\mathcal{M}} = (\mathcal{M}/\mathcal{M}(0) - 1) \times 100\%$. The program starts with a withdrawal phase of 60 days, cycling then begins where each cycle extends over a 6–month period. Only the first two cycles are shown, however, simulations are conducted for a 40–year time period, i.e. 80 cycles.

Since there are no available COMSOL modules that couples computational fluid dynamics with the two–phase percolation and diffusion in porous media, the available general forms of the coefficient Partial Differential Equations (cPDE), of the domain Ordinary Differential Equations (dODE), and of the boundary Ordinary Differential Equations (bODE), are used to solve our systems of equations in a coupled thermo–hydraulic framework. COMSOL gives analytical expressions to track the evolution of the hydrogen viscosity μ_γ, thermal conductivity Λ_γ, and heat capacity $C_{p\gamma}$ as functions of temperature (see Appendix B). Other van Genuchten, thermal, and hydraulic parameters are detailed in Table (1).

4. Parametric study

Due to the lack of any experimental data treating hydrogen invasion into the rock salt, this parametric study is presented before performing simulations on the cavern scale. The objective of this section is to investigate the effect of van Genuchten parameter (P_r) and hydrogen–brine diffusion coefficient ($\bar{D}_{h\lambda}$) on the percolation–diffusion phenomenon. The chosen van Genuchten parameter and diffusion coefficient values will then be used in a real–scale cavern simulations, and while assuming a pessimistic or an overestimating scenario with regard to the total mass of lost hydrogen. To simplify the calculations, this study is performed for a one–dimensional axisymmetric transient boundary value problem (Fig. 3(a)).

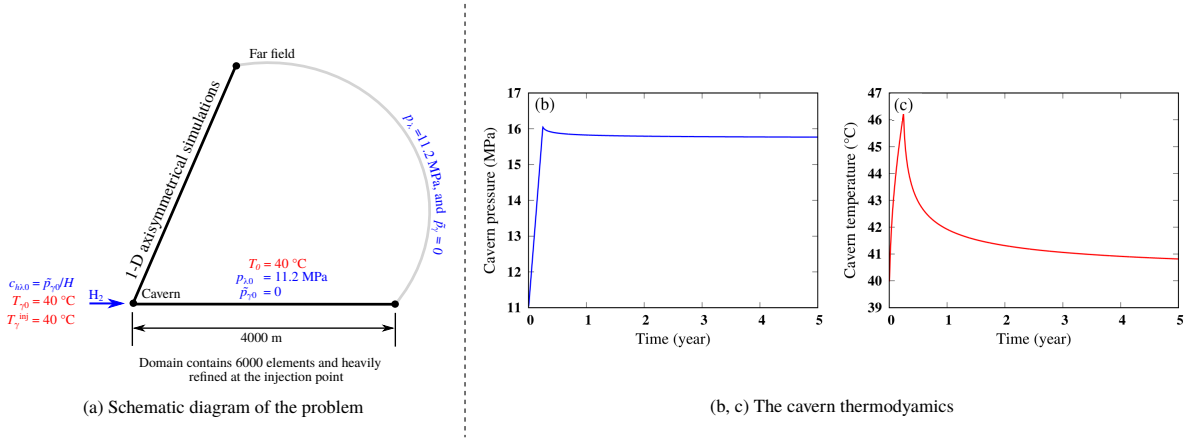

Figure 3: (a) Schematic diagram representing the transient boundary value problem to perform the parmetric study of hydrogen invasion into a saturated rock salt. The cavern volume averaged (b) pressure, and (c) temperature. Injection continues through 90 days, it then stops allowing for heat transfer and hydrogen mass exhange with the rock salt.

Initial and boundary conditions are set similar to the working conditions of the spherical cavern (Fig.

Table 1: Hydraulic, thermal, and van Genuchten parameters to model hydrogen invasion into the rock salt.

Interpretation	Parameter (unit)	Value	Reference
Rock salt permeability	k (m^2)	1×10^{-20}	[45, 46]
Rock salt porosity	n	0.01	[45, 46]
Brine density	ρ_λ ($\mathrm{kg/m}^3$)	1200	[29]
Brine isochoric compressibility	$\chi_{T\lambda}$ (1/Pa)	46×10^{-11}	[29]
Brine isobaric expansivity	$\chi_{p\lambda}$ (1/K)	45×10^{-5}	[29]
Brine dynamic viscosity	μ_λ (Pa s)	1.32×10^{-3}	[29]
Brine thermal conductivity	Λ_λ (W/m/K)	0.51	[29]
Brine heat capacity	$C_{p\lambda}$ (J/kg/K)	3300	[29]
Rock salt pore pressure	p_λ (Pa)	$-\rho_\lambda \, \mathtt{g} \, z$	Overestimating study
Rock salt density	ρ_σ ($\mathrm{kg/m}^3$)	2200	[47]
Rock salt thermal conductivity	Λ_σ (W/m/K)	6	[47]
Rock salt heat capacity	$C_{p\sigma}$ (J/kg/K)	900	[47]
Maximum brine saturation	$S_{\lambda s}$	1.0	Assumed
Residual brine saturation	$S_{\lambda r}$	0.15	[39]
van Genuchten parameter	P_r (Pa)	8×10^6 or 15×10^6	Parametric study
van Genuchten parameter	ℓ	0.5	[48]
Mass creation terms	π_b and π_h ($\mathrm{kg/m}^3\mathrm{/s}$)	0	Assumed
Hydrogen mass concentration	$c_{h\lambda}$	$\tilde{p}_\gamma / H$	Definition
Hydrogen diffusion in brine	$\bar{D}_{h\lambda}$ ($\mathrm{m}^2\mathrm{/s}$)	5×10^{-7} or 5×10^{-10}	Parametric study
Diffusion correction parameter	q	2.1	[21]
Henry's constant hydrogen–brine	K_H (L atm/mol)	1300	[49, 50]

2(a)). Hydrogen concentration is initially neglected in the rock domain ($c_{h\lambda} = 0$). Consequently, the initial rock salt pseudo–hydrogen pressure is assumed equal to zero ($\tilde{p}_{\gamma 0} = 0$). The initial rock salt interstitial brine pressure is set equal to the halmostatic value $p_{\lambda 0} = 11.2$ MPa. The cavern (injection point) is initially assumed in thermal equilibrium with the surrounding rock domain at $T = 40$ °C. The cavern is filled gradually with hydrogen during a 90–day time period, where the cavern pressure is increased from halmostatic to ∼16 MPa (around the maximum cycling value of the real cavern (Fig. 9(a)). Injection then stops and hydrogen is left to diffuse and/or percolate into the rock domain. Figures 3(b, c) show the hydrogen pressure and temperature within the cavern during a 5–year time period.

During filling, the cavern averaged temperature increases from 40 °C to ∼46.2 °C. Heat exchange with the colder surrounding rock salt is observed in Fig. 3(c) during 5 years. To simulate the two–phase

hydrogen percolation into the rock salt, the van Genuchten parameter $\ell = 0.5$ is used as cited in a few articles for rock salt [48]. Similar works have used a van Genuchten parameter $P_r \in [10 - 15]$ MPa for air and nitrogen percolations in concrete, granite, or crushed rock salt [39, 48, 51]. For this study, simulations are performed for $Pr = 8$ and 15 MPa. The residual saturation $S_{\lambda r} = 0.15$ is used as in *Mahjoub et al.* [39] and *Poppei et al.* [48]. The possibility to have a fully brine saturated state is taken into consideration by setting $S_{\lambda s} = 1$. To investigate the effect of Fickian diffusion on the total hydrogen mass lost into the rock salt, a wide range (3 orders of magnitude) of diffusion coefficient is considered, i.e. $\bar{D}_{h\lambda} = 5 \times 10^{-7}$ or 5×10^{-10} m^2/s. Consequently, four simulations are performed: for $P_r = 8$ MPa and $\bar{D}_{h\lambda} = 5 \times 10^{-7}$ or 5×10^{-10} m^2/s; and for $P_r = 15$ MPa and $\bar{D}_{h\lambda} = 5 \times 10^{-7}$ or 5×10^{-10} m^2/s. Results are simultaneously correlated and analyzed.

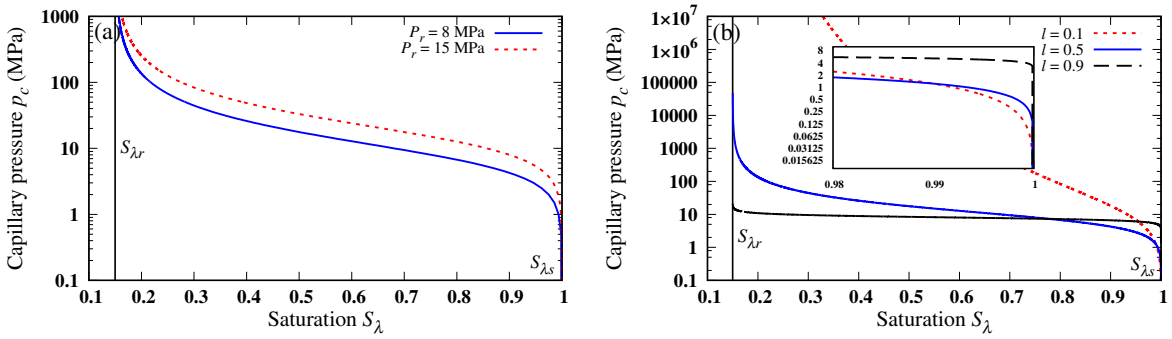

Figure 4: Capillary pressure as calculated by the van Genuchten equation (Eq. 5), (a) for $\ell = 0.5$ and $P_r = \{8, 15\}$ MPa, and (b) for $P_r = 8$ MPa and $\ell = \{0.1, 0.5, 0.9\}$.

Figure 4(a) shows the brine saturation evolution as function of the capillary pressure for the two values of the van Genuchten parameter P_r. It is obvious that a tremendous cavern pressure is needed for hydrogen to invade the rock salt in a pure or even a semi–pure nature ($S_\lambda < 0.15$). For typical working conditions of our typical spherical cavern, capillary pressure ranges between 0 and ~ 4 MPa. Consequently, hydrogen saturation in the pore brine is expected to be very low (< 0.05), i.e. $S_\lambda > 0.95$. It is also observed that a lower value of the parameter P_r allows for a more significant percolation of hydrogen for the the same capillary pressure.

Figure 5 shows the rock salt radial profiles of pseudo–hydrogen pressure, of brine pore pressure, and of temperature for the transient boundary value problem of Fig. 3(a). Hydrogen exists only in the domain where the pseudo–pressure is grater than zero ($S_\lambda < 1$). It is observed that the rock domain temperature is minimally affected by the choice of the diffusion coefficient and the van Genuchten parameter P_r (Figs 5(c, f)). Figs 5(b, e) show that the rock salt brine pressure is also independent of the value of the diffusion coefficient. However, the van Genuchten definition (Eq. 5) necessitates that the brine pore pressure be dependent of the parameter P_r. Comparing Figs 5(a, d) demonstrates that the percolation is slightly affected by the value of the diffusion coefficient. For instance, for both values of $\bar{D}_{h\lambda}$, hydrogen percolates

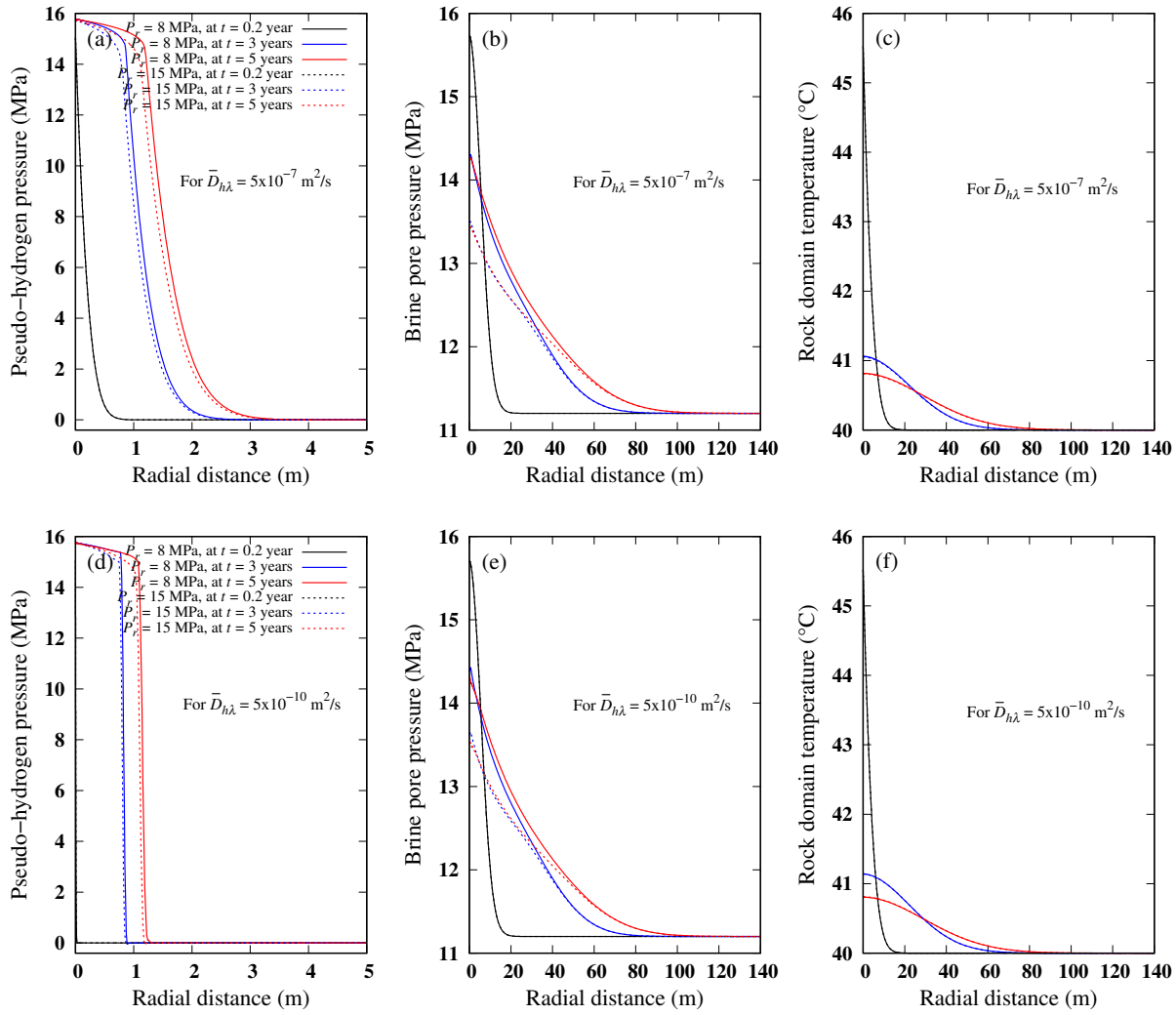

Figure 5: (a, d) Pseudo-hydrogen pressure, (b, e) brine pore pressure, and (c, f) rock salt temperature radial profiles at three distinct times of 0.2, 3, and 5 years. These profiles are traced within the rock domain and shown for the four permutations of P_r and $\bar{D}_{h\lambda}$ values.

to a distance of almost ∼1.3 m after 5 years. However, when the diffusion coefficient value is significant, percolation continues to show a diffusive nature where the affected domain could reach a distance of ∼3 m after 5 years. Before percolation takes place ($t < 89$ days (Fig. 6(a))), the chosen value of P_r has no effect on the hydrogen pressure profiles in the rock domain (see the black curves in Figs 5(a, d)). As expected, it is seen that smaller values of the parameter P_r allow for more percolation of hydrogen (compare red and blue curves of Figs 5(a, d)).

Figure 6 shows the histories of the brine saturation at the cavern wall, of the percolated and of the Fickian diffused hydrogen masses into the rock salt domain. The exchanged masses are calculated by integrating Eq. 9 over time and over a surface equivalent to that of the cavern in Fig. 2(a).

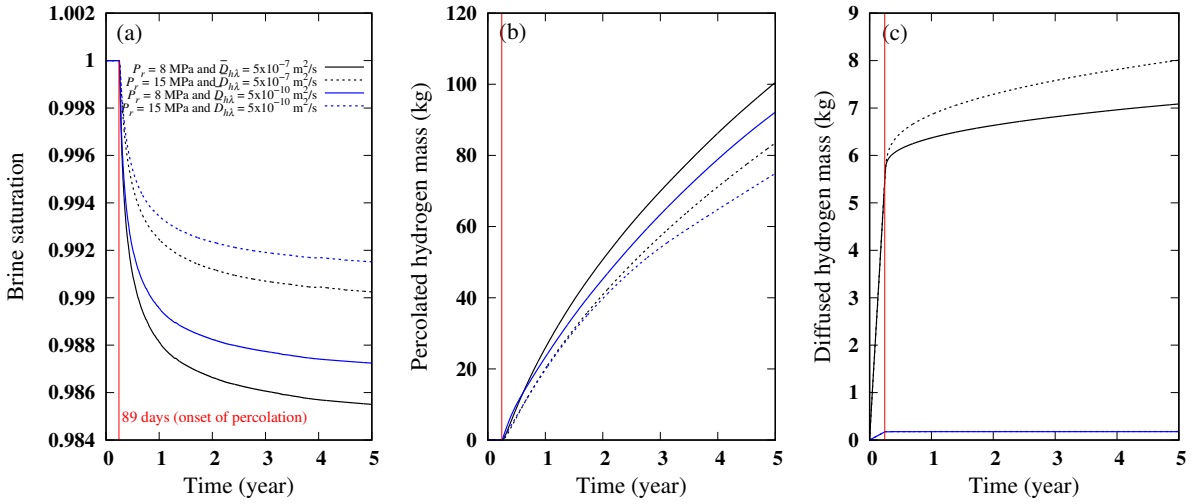

Figure 6: (a) Brine saturation history at the cavern wall, (b) two–phase percolated hydrogen mass history, and (c) Fickian diffused hydrogen mass history. Histories are shown for the four permutations of P_r and $\bar{D}_{h\lambda}$ values.

Figure 6(a) shows that the two–phase percolation starts after almost ∼89 days. Due to the low capillary pressure, i.e. $p_c \in [2-3]$ MPa, the brine saturation is very slightly altered (minimum of ∼0.985). Figure 6(b) shows the hydrogen mass percolated into the rock salt domain. Obviously, a more significant diffusion coefficient and a smaller P_r value allow for a more percolated mass into the rock salt, which translates into a lesser brine saturation. Unlike percolation, hydrogen starts to diffuse into the rock salt domain as soon as a hydrogen pressure gradient is established between the cavern and the rock domain (Fig. 6(c)). It is also noticed that the Fickian diffusion is significant before percolation. However, as soon as percolation starts, hydrogen replaces brine by a certain saturation which creates two phases, and the Fickian diffusion rate becomes very slow. One can also see that hydrogen diffuses more for a greater value of the parameter P_r. Actually, a larger P_r indicates a less percolation which promotes the Fickian diffusion. This remark is strengthened by noticing that the deviation of the black curves of Fig. 6(c) takes place instantly with percolation, i.e. $t \approx 89$ days. This conclusion is less obvious when the diffusion coefficient is very low (blue curves of Fig. 6(c)).

Though a value of $\ell = 0.5$ has been used in literature for two–phase flow in rock salt, it is intriguing to investigate the effect of this parameter on the percolation and diffusion of hydrogen. Henceforth, for $P_r = 8$ MPa, Fig. 4(b) shows the brine saturation as function of the parameter ℓ. It is conceivable and expected that the percolation depends on the value of ℓ, however, this dependency becomes less significant for a quite low hydrogen saturation, i.e. $S_\lambda \approx 0.98$ (see the zoom–in of Fig. 4(b)). When ℓ approaches 0.9, the capillary pressure exceeds 4 MPa, which is translated into no percolation at all for the working and boundary conditions of this one–dimensional problem (Fig. 7(a)).

Figure 7 shows the percolated and diffused hydrogen masses for $P_r = 8$ MPa, $\bar{D}_{h\lambda} = 5 \times 10^{-7}$ m^2/s, and $\ell = \{0.1, 0.5, 0.9\}$. Reducing ℓ to 0.1 increases the percolated mass by 2.65 folds. However, no percolation is observed for $\ell \approx 0.9$.

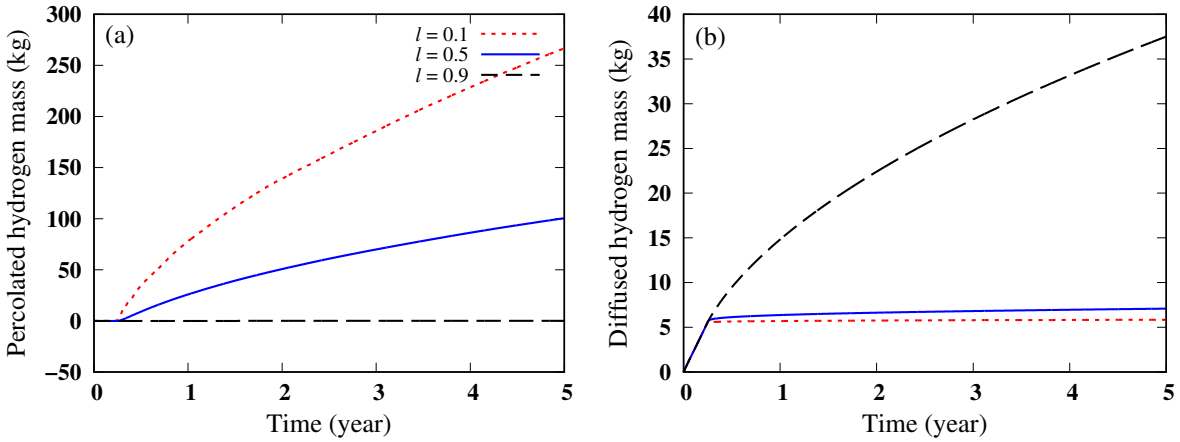

Figure 7: (a) Percolated and (b) diffused hydrogen masses through 5 years for $P_r = 8$ MPa, $\bar{D}_{h\lambda} = 5 \times 10^{-7}$ m^2/s, and $\ell = \{0.1, 0.5, 0.9\}$.

As expected, when there is no percolation, hydrogen diffuses the most (black curve of Fig. 7(b)). For $\ell = \{0.1, 0.5\}$, Fickian diffusion gets affected by the percolation and its parabolic behavior changes as soon as percolation starts (blue and red curves of Fig. 7(b)). Percolation happens a bit earlier for $\ell = 0.1$, which is attributed to a lower capillary pressure for the same saturation (see the zoom–in of Fig. 4(b) for $S_\lambda \in [0.99 - 1]$). For the coming stimulations on the cavern scale, we will assume van Genuchten parameters of $P_r = 8$ MPa, of $\ell = 0.5$, and a hydrogen–brine diffusion coefficient of $\bar{D}_{h\lambda} = 5 \times 10^{-7}$ m^2/s.

5. Cavern–scale cycling simulations

A two–dimensional axisymmetric model was adopted to simulate heat and mass exchange with the surrounding rock domain during hydrogen cycling in the real cavern (Fig. 2(a)). Figure 8 shows the spatial discretization of the rock domain. The cavern is not discretized since a uniform thermodynamic state is assumed within the cavern. Initial and boundary conditions are displayed on the graph.

Figures 9(a, b) show the cavern averaged temperature and pressure as function of cycling. Hydrogen pressure is not showing any changes during cycling as the cavern volume is assumed constant. However, temperature is showing some changes due to the energy exchanged with the surrounding rock salt domain.

Figure 9(c) shows the hydrogen pseudo–capillary pressure averaged over the cavern surface during cycling. The behavior of the capillary pressure becomes almost identical after five cycles. The capillary pressure does not exceed 2 MPa for the working and boundary conditions of this typical spherical cavern.

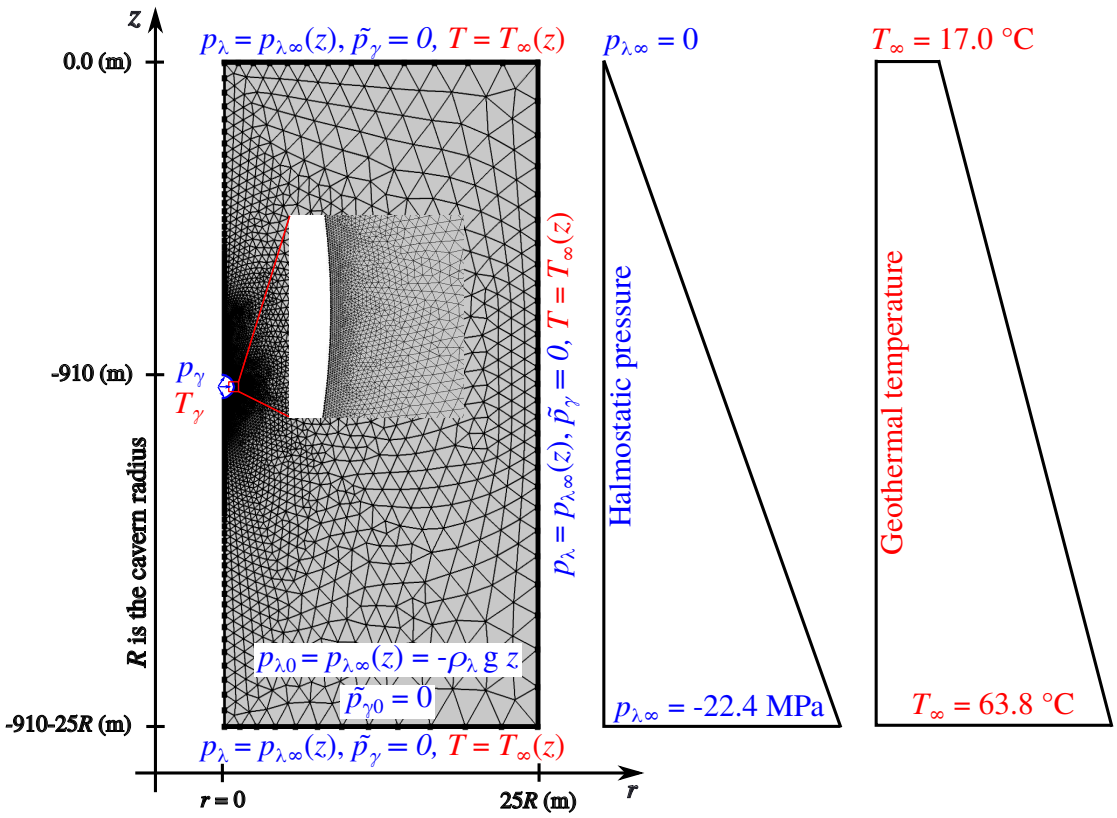

Figure 8: A two–dimensional axisemtric discretization of the boundary value problem of Fig. 2(a). A surrounding rock volume of $25R$ is chosen around the cavern to avoid the effect of far–field boundaries. Mesh is considerably refined close to the cavern wall to account for abrupt changes/large gradients. Mesh contains 160113 triangular elements.

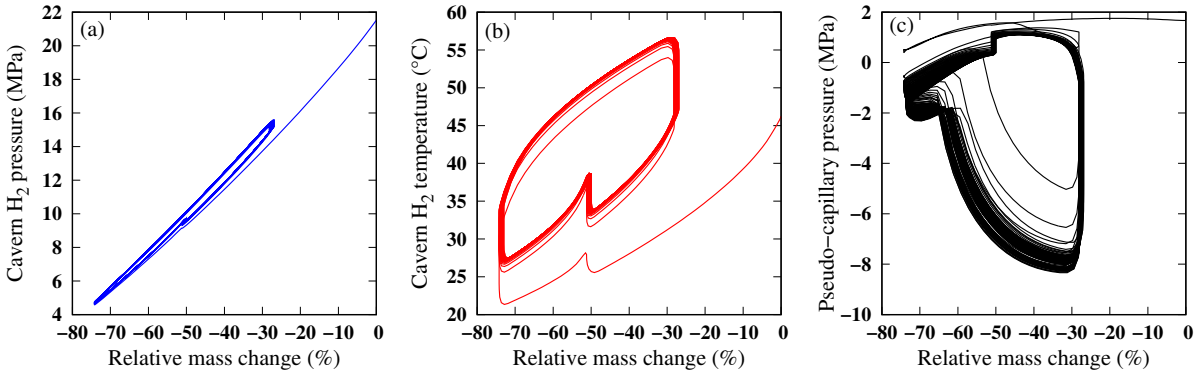

Figure 9: (a) cavern average pressure, (b) cavern average temperature, and (c) hydrogen pseudo–capillary pressure averaged over the cavern surface. The three quantities are presented as function of cycling/relative mass changes within the cavern.

To study the hydrogen mass exchanged with the rock domain, Fig. 10(a) shows the brine saturation, and Fig. 10(b) shows the radial component of hydrogen filtration velocity averaged over the cavern surface during the first four cycles. Other cycles are not displayed due to similarity and to avoid redundant

repetitions.

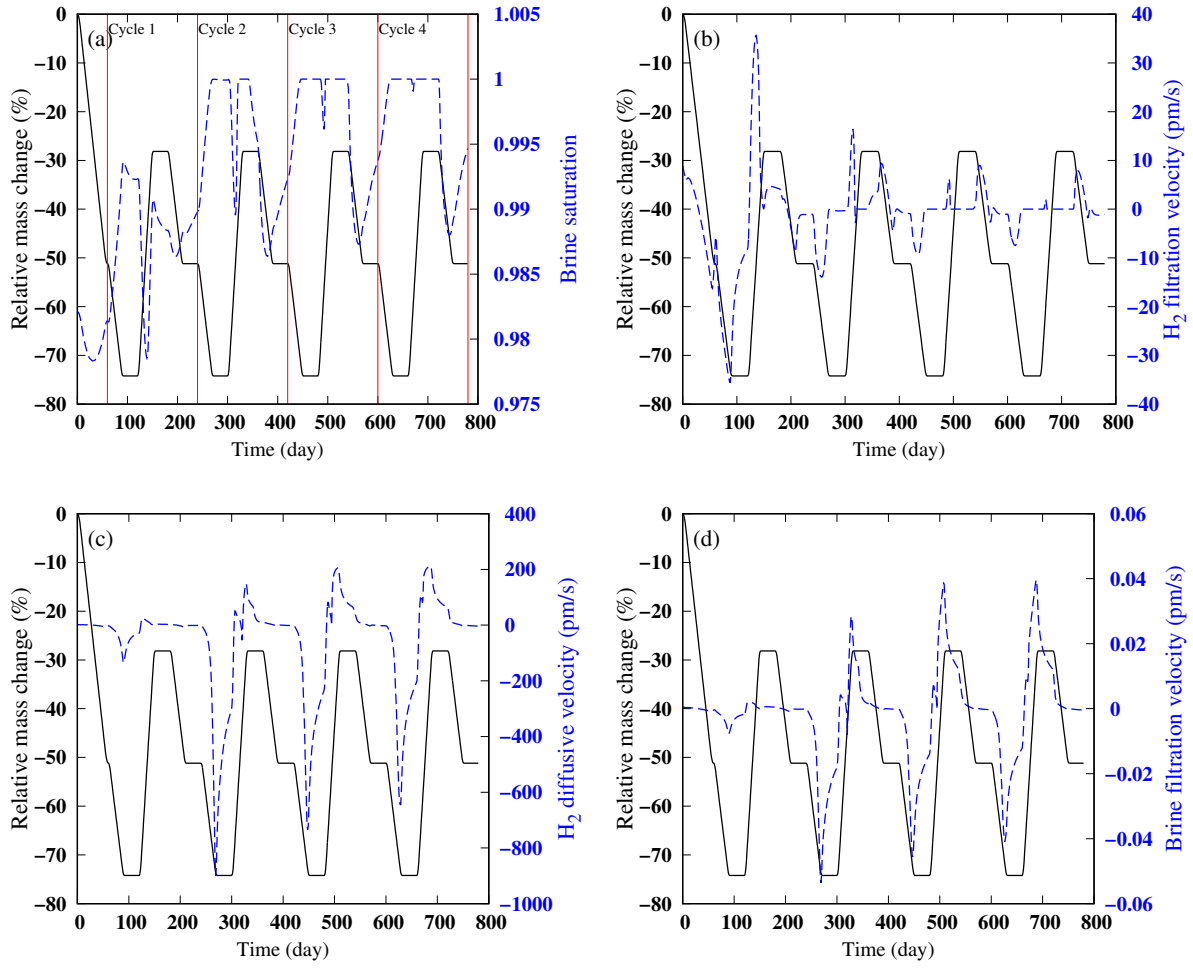

Figure 10: (a) Brine saturation at the cavern wall, as well as the surface averaged radial components of (b) the hydrogen filtration velocity, (c) the Fickian diffusive velocity, and (d) the brine filtration velocity during the first four cycles.

The debrining and the standstill phases of 180 days (Sect. 3.3) have led the brine saturation at the cavern wall to decrease to ∼0.981 before any cycling (Fig. 10(a)). The subsequent withdrawal has counteracted this reduction in the brine saturation by allowing the percolated hydrogen to leave back to the cavern volume, and again a full brine saturation is reached. Furthermore, hydrogen would percolate into and leave from the rock domain as a function of the cavern hydrogen pressure (Fig. 10(b)). This allows for a reduction in the brine saturation at the cavern wall before it sustains the full saturation state (Fig. 10(a) and Fig. 11(a)).

The Fickian diffusive velocity resembles the brine filtration velocity (Figs 10(c, d)). Depending on the direction of hydrogen pressure gradient, hydrogen may diffuse into the rock domain, or pour down the cavern wall along with the leaving brine. The surface averaged radial component of the brine filtration

velocity is show in Fig. 10(d). It is observed that brine moves into the cavern volume when the percolated hydrogen leaves the rock domain and vice versa. Besides, the thermal effects are noticed on the behavior of the brine filtration and the Fickian diffusive velocities due to the hydro–thermal coupling, especially during the standstill phases.

To understand how the rock domain interstitial brine gets drained by the invading hydrogen, Fig. 11(a) shows the time variations of the brine saturation and the pseudo–capillary pressure at the cavern wall for the first four cycles.

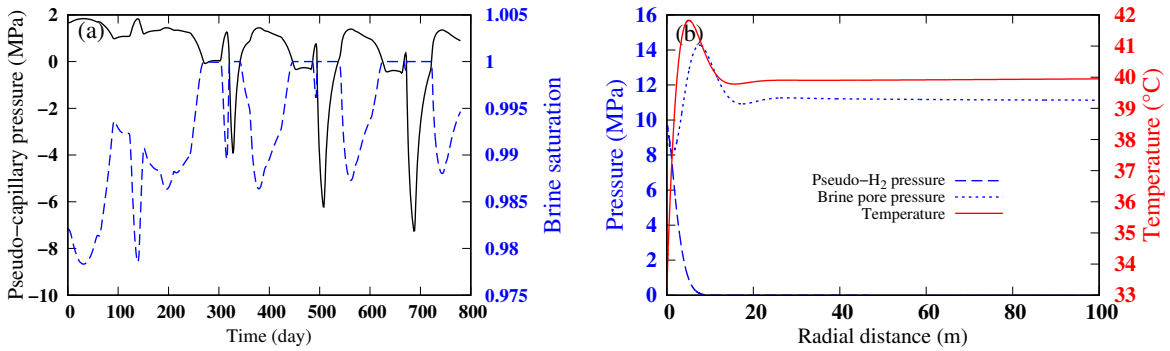

Figure 11: (a) Time variations of the cavern surface averaged brine saturation and pseudo–capillary pressure for the first four cycles. (b) Radial profiles of interstitial brine pressure, of hydrogen pseudo–pressure, and of temperature within the rock domain at the end of cycling/at 40 years.

One can see that hydrogen percolates into the rock domain when the capillary pressure is positive. Besides, the hydrogen saturation rate (increasing or decreasing) has the same sign as the capillary pressure rate.

To study the zone disturbed by brine pore pressure changes, hydrogen pseudo–pressure and temperature fluctuations, Fig. 11(b) shows the radial profiles of these variables at the end of cycling, i.e. 40 years. The altered zone due to hydrogen invasion into the rock domain has not exceeded ∼15 m after 40 years of seasonal cycling. However, this zone extends to ∼40 m due to brine pore pressure and rock domain temperature changes. Knowing the range of these distances helps design a network of underground caverns while avoiding harmful interactions.

Figure 12 shows the hydrogen mass exchanged with the surrounding rock domain due to two–phase percolation and the Fickian diffusion. Figure 12(a) is a zoom–in of Fig. 12(b) for the first four cycles/800 days.

Both the percolated and diffused hydrogen masses tend to reduce during withdrawal in accordance with Figs 10(b, c). Even–though the Fickian diffused mass is initially smaller than the percolated mass, after ∼25 years of cycling, the diffused mass becomes more significant than the two–phase percolated mass (Fig. 12(b)). Eventually, the percolated and the diffused hydrogen masses summed up to ∼93 kg

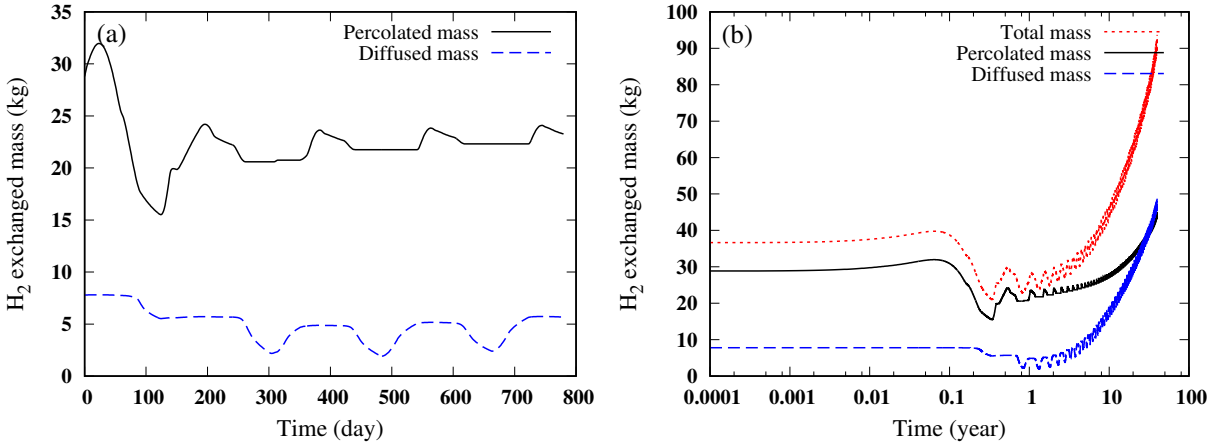

Figure 12: Darcian percolated and Fickian diffused hydrogen masses during 40 years of cycling. Figure (a) is a zoom–in of figure (b) for the first four years. The debrining and the standstill phases of 180 days (Sect. 3.3) have led to the initial percolated and diffused masses observed in figure (a).

after 40 years of the cavern operation.

6. Discussion

For a P_r range that resembles the hydrogen invasion into the rock salt, Sect. 4 has shown that the Darcian percolation has a slight dependency on the value of P_r. The parameter ℓ has been assigned a value of 0.5 for rock salt in a few research papers. However, possible high values ($\ell \sim 0.9$) can increase considerably the capillary pressure at full brine saturation leading to a naught percolation. A value of $\ell = 0.1$, close to the lowest limit, has increased the hydrogen mass percolated into the rock salt domain by 3 folds (Fig. 7(b)).

The value of the diffusion coefficient $\bar{D}_{h\lambda}$ does not affect directly the Darcian percolation, but rather its diffusive nature. Percolation becomes more of a piston–like for very small values. Consequently, hydrogen mass lost due to percolation differed a little bit depending on the diffusion coefficient value (Fig. 6(b)). However, it is natural that the hydrogen mass lost due to Fickian diffusion is almost 50 times larger for a 3–order of magnitude higher diffusion coefficient (Fig. 6(c)).

The simulations on the cavern scale have been performed such that an overestimating/a pessimistic scenario of lost hydrogen is considered. Therefore, while setting $\ell = 0.5$, values of $P_r = 8$ MPa and $\bar{D}_{h\lambda} = 5 \times 10^{-7}$ m^2/s have been chosen. Cycling simulations prove that percolation happens mostly when the cavern pressure is close to the maximum cycling value, i.e. $p_\gamma \approx 16$ MPa. Yet, depending on the sign of the pressure gradient, hydrogen may percolate into/leave from the rock domain. The Fickian diffusion resembles the brine filtration, following the pressure gradient direction, hydrogen tends to diffuse into the rock domain or pours down the cavern wall along with the leaving brine. Eventually, the total

mass of lost hydrogen sums up to ∼93 kg. This mass is extremely negligible compared to the hydrogen mass manipulated during one cycle ($\mathcal{M} = 2.05$ Mkg), i.e. the percentage of the lost mass to one cycle mass is $\sim 0.005\%$.

Though a wide range of model parameters is studied, our research rests limited to its numerical nature. A laboratory validation is needed. We assume a homogeneous rock salt all around the spherical cavern. However, rock salt can be widely heterogeneous. Besides, this research does not introduce any permeable interlayers, nor does it account for damaged zones. The implementation of heterogeneities in rock salt, whether in the mechanical or the hydraulic properties, affects the transported/exchanged quantity of hydrogen. This effect can be direct as in the case of increased permeability, or indirect as in the case of weaker or more damageable rock salt.

The available research concerning gas migration in rock salt promotes the results found in our research. For instance *Jockwer and Wieczorek* [53] have stated that the presence of a damaged zone (DRZ) is the main factor for gas transport in rock salt. They conducted experiments and simulations concerning helium, neon, and butane. They found that the diffusion coefficient of these gases increased by two orders of magnitude in the DRZ. Out of the DRZ, the measured permeabilities were in the order of 10^{-19} and 10^{-20} m^2, and the pseudo gas pressure slightly penetrated the rock salt in a two–phase psiton–like flow (compare to Fig. 5(d)). *Senger et al.* [51] studied gas (particularly air) migration in concrete. They have found that the gas penetrated distances were limited to 1.5 m after 4 years of injection (compare to Fig. 5(a, d)). The two–phase gas saturation depended on the permeabilities, yet it was less than 0.1 for permeabilities in the order of 10^{-19} m^2. Generally, the existed literature already confirms that permeable interlayers are the main transport conduits around salter caverns [10, 11].

7. conclusion and perspectives

In general, for an overly assumed diffusion of hydrogen in brine ($\bar{D}_{h\lambda} = 5 \times 10^{-7}$ m^2/s) [52], a null pressure entry, and overestimating van Genuchten parameters, the hydrogen mass lost to the rock domain remains very negligible. Yet, increasing energy demands necessitate fast utilization of underground caverns. The severe utilization of salt caverns exposes them to considerable pressure and temperature changes throughout short periods, which may affect the development of the damaged zones . The introduction of a damaged zone, during cycling and at the end of leaching, can affect the total mass of the lost hydrogen. Future studies will include, in a first step, laboratory work to develop mass transport laws that would describe precisely hydrogen migration into the rock salt. In a second step, constitutive laws that quantify the permeability and porosity evolutions of rock salt due to mechanical, hydraulic and thermal charges would be needed. Once these transport and constitutive laws are developed, they can be integrated in our current frame work to estimate their effect on hydrogen percolation and diffusion

during rock salt damaging/severe exploitation of caverns.

Though our simulations have demonstrated that cycling reduces the total amount of transported hydrogen (Fig. 12(b)), the role of heterogeneities, whether mechanical or hydraulic, needs also to be investigated in a future research. Moreover, in a laboratory hydrogen storage model, we are currently investigating the importance of other fluxes, F_2, F_3, and F_1 of Fig. 1; F_1 is expected to have an impact on the hydrogen thermodynamic behavior. Once these fluxes are quantified, their payoffs should be compared and/or added to the flux F_4, presented in this research, to draw a general conclusion about the hydrogen–tightness of salt caverns.

8. Acknowledgment

Authors would like to thank Géodénergies and the French Association Nationale de Recherche (ANR) for their financial support via the two projects: ROSTOCK–H; and STOPIL–H.

Appendix A.

Real hydrogen state law

A real gas behavior is assumed in our simulations of hydrogen storage and migration into the rock salt. The hydrogen state equation can be completely described using two state functions; the mass density $\rho_\gamma(p_\gamma, T_\gamma)$, and the heat capacity $C_{p_\gamma}(T_\gamma)$ at a given pressure [37]. The thermodynamic variables are related to each other through the formula,

$$\rho_\gamma = \frac{p_\gamma}{T_\gamma Z}, \tag{A.1}$$

with Z being the hydrogen compressibility factor. Equation A.1 can be written in a derivative form as,

$$\frac{d\rho_\gamma}{\rho_\gamma} = \chi_{T\gamma}\, dp_\gamma - \chi_{p\gamma}\, dT_\gamma, \tag{A.2}$$

with $\chi_{T\gamma}$ being the hydrogen isochoric compressibility and $\chi_{p\gamma}$ the hydrogen isobaric thermal expansivity. Integrating Eq. A.2 gives,

$$\ln\left(\frac{\rho_\gamma}{\rho_{\gamma 0}}\right) = \int_{p_{\gamma 0}}^{p_\gamma} \chi_{T\gamma}\, dp_\gamma - \int_{T_{\gamma 0}}^{T_\gamma} \chi_{p\gamma}\, dT_\gamma, \tag{A.3}$$

which can be written as,

$$\rho_\gamma = \rho_{\gamma 0} \exp\left(\int_{p_{\gamma 0}}^{p_\gamma} \chi_{T\gamma}\, dp - \int_{T_{\gamma 0}}^{T_\gamma} \chi_{p\gamma}\, dT_\gamma\right), \tag{A.4}$$

with $\rho_{\gamma 0}$, $p_{\gamma 0}$, and $T_{\gamma 0}$ being the hydrogen density, pressure, and temperature at the reference state. Both $\chi_{T\gamma}$ and $\chi_{p\gamma}$ are functions of the thermodynamic variables, i.e. $\chi_{T\gamma} = \chi_{T\gamma 0}\,(p_\gamma/p_{\gamma 0})^{b_T}$, and $\chi_{p\gamma} = \chi_{p\gamma 0}\,(T_\gamma/T_{\gamma 0})^{a_p}$, with $\chi_{T\gamma 0}$ and $\chi_{p\gamma 0}$ being the values of $\chi_{T\gamma}$ and $\chi_{p\gamma}$ at the reference state respectively, and b_T and a_p are dimensionless constants. Once the reference state is fixed, Eq. A.4 can be extended to,

$$\rho_\gamma = \rho_{\gamma 0} \exp\left(p_{\gamma 0}\frac{\chi_{T\gamma 0}}{1+b_T}\left[\left(\frac{p_\gamma}{p_{\gamma 0}}\right)^{1+b_T} - 1\right] - T_{\gamma 0}\frac{\chi_{p\gamma 0}}{1+a_p}\left[\left(\frac{T_\gamma}{T_{\gamma 0}}\right)^{1+a_p} - 1\right]\right). \tag{A.5}$$

A high accuracy equation of state was used in our simulations [54]. Once the model parameters are known, Eq. A.5 can be fed to COMSOL where a real thermodynamic behavior of hydrogen is solved for.

The reference state is set to $(p_{\gamma 0}, T_{\gamma 0}, \rho_{\gamma 0}) = (1.0\ \text{MPa}, -100\ ^\circ\text{C}, 1.391\ \text{kg/m}^3)$, then for a temperature range of $T_\gamma \in [-100 \text{ to } 100]\ ^\circ\text{C}$, and a pressure range of $p_\gamma \in [1 \text{ to } 25]$ MPa, the following values of model parameters fitted best the data of *Kunz and Wagner* [54]: $\chi_{T\gamma 0} = 1.04562$ (1/MPa); $\chi_{p\gamma 0} = 5.4738 \times 10^{-3}$ (1/K); $b_T = -1.05526$; and $a_p = -1.002851$. Figure A.1 shows the relative error (ε_ρ) in the hydrogen density as calculated by *Kunz and Wagner* [54] and by Eq. A.5.

The range of pressure and temperature changes during the cavern cycling (Figs 9(a, b)) is displayed on Fig. A.1, where the error percentage in the calculated hydrogen density does not exceed 5.0%.

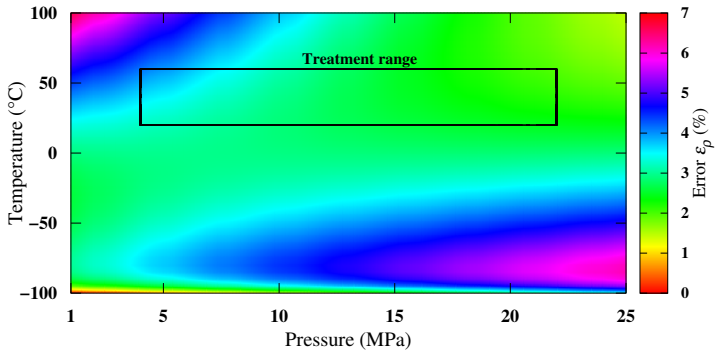

Figure A.1: Relative error (ε_ρ) in the hydrogen density as calculated by *Kunz and Wagner* [54] and by Eq. A.5.

Appendix B.

COMSOL equations

COMSOL gives analytical expressions to track the evolution of hydrogen dynamic viscosity μ_γ, thermal conductivity Λ_γ, and heat capacity $C_{p\gamma}$ as functions of temperature. During hydrogen cycling, for $T_\gamma \in [290 - 235]$ K, the dynamic viscosity changes as,

$$\mu_\gamma = 2.14524642 \times 10^{-6} + 2.54245 \times 10^{-8}\, T_\gamma - 1.0235587 \times 10^{-11}\, T_\gamma^2 + 2.80895021 \times 10^{-15}\, T_\gamma^3, \quad \text{(B.1)}$$

the thermal conductivity changes as,

$$\Lambda_\gamma = 0.00517975922 + 6.72778 \times 10^{-4}\, T_\gamma - 3.0388973 \times 10^{-7}\, T_\gamma^2 + 6.58874687 \times 10^{-11}\, T_\gamma^3, \quad \text{(B.2)}$$

and the heat capacity changes as,

$$C_{p\gamma} = 10808.501 + 21.5799904\, T_\gamma - 0.0444720318\, T_\gamma^2 + 3.85401176 \times 10^{-5}\, T_\gamma^3 - 1.14979447 \times 10^{-8}\, T_\gamma^4. \quad \text{(B.3)}$$

References

[1] Lattin C. W. and Utgikar P. V. (2007). Transition to hydrogen economy in the United States: A 2006 status report. International Journal of Hydrogen Energy, 32: 3230–3237.

[2] McPherson M., Johnson N., and Strubegger M. (2018). The role of electricity storage and hydrogen technologies in enabling global low-carbon energy transitions. Applied Energy, 216: 649–661.

[3] Caglayan D. G., Weber N., Heinrichs H. U., Linßen J., Robinius M., Kukla P. A., and Stolten D. (2020). Technical potential of salt caverns for hydrogen storage in Europe. International Journal of Hydrogen Energy, 45: 6793–6805.

[4] Deveci M. (2018). Site selection for hydrogen underground storage using interval type–2 hesitant fuzzy sets. International Journal of Hydrogen Energy, 43(19): 9353–9368.

[5] Lehner M., Tichler R., Steinmüller H., and Koppe M. (2014). Power–to–gas: technology and business models. Springer.

[6] Götz M., Lefebvre J., Mörs F., Koch A. M., Graf F., Bajohr S., Reimert R., and Kolb T. (2016). Renewable Power-to-Gas: A technological and economic review. Renewable Energy, 85: 1371–1390.

[7] Iordache M., Schitea D., Deveci M., Akyurt I. Z., and Iordache I. (2019). An integrated ARAS and interval type-2 hesitant fuzzy sets method for underground site selection: Seasonal hydrogen storage in salt caverns. Journal of Petroleum Science and Engineering, 175: 1088–1098.

[8] Ozarslan A. (2012). Large–scale hydrogen energy storage in salt caverns. International Journal of Hydrogen Energy, 37(19): 14265–14277.

[9] Pamucar D., Deveci M., Schitea D., Erişkin L., Iordache M., and Iordache I. (2020). Developing a novel fuzzy neutrosophic numbers based decision making analysis for prioritizing the energy storage technologies. International Journal of Hydrogen Energy, 45(43): 23027–23047.

[10] Liu W., Zhang Z., Chen J., Jiang D., Wu F., Fan J., and Li Y. (2020). Feasibility evaluation of large–scale underground hydrogen storage in bedded salt rocks of China: A case study in Jiangsu province. Energy, 198: 117348.

[11] Liu W., Chen J., Jiang D., Shi X., Li Y., Daemen J.J.K., and Yang C. (2016). Tightness and suitability evaluation of abandoned salt caverns served as hydrocarbon energies storage under adverse geological conditions (AGC). Applied Energy, 178: 703–720.

[12] Bechtel A., Savin S. M., and Hoernes S. (1999). Oxygen and hydrogen isotopic composition of clay minerals of the Bahloul Formation in the region of the Bou Grine zinc–lead ore deposit (Tunisia):

evidence for fluid–rock interaction in the vicinity of salt dome cap rock. Chemical Geology, 156: 191–207.

[13] Amaziane B., Keko A. Ž., and Jurak M. (2014). Modeling compositional compressible two–phase flow in porous media by the concept of the global pressure. Computational Geosciences, 18(3–4): 297–309.

[14] Yortsos Y. C., Xu B., and Salin D. (1997). Phase diagram of fully developed drainage in porous media. Physical Review Letters, 79(23): 4581–4584.

[15] Lenormand R. (1989). Flow through porous media: limits of fractal patterns. Proceedings of the Royal Society A, 423(1864): 159-168.

[16] Charnavel Y., Leca D., and Poulain F. (1983). Advanced geometrical modelling of salt dissolution during cavern leaching – illustration with a case study. *In*: The SMRI Meeting, Las Vegas, Nevada, USA.

[17] Pernette E. and Dussaud M. (1983). Underground storages at Tersanne and Etrez: prediction and simulation of cavity leaching in a salt layer charged with insoluble materials. *In*: The sixth International Symposium on Salt, Toronto, Canada.

[18] Caglayan D. G., Weber N., Heinrichs H. U., Linßen J., Robinius M., Kukla P. A., and Stolten D. (2020). Technical potential of salt caverns for hydrogen storage in Europe. International Journal of Hydrogen Energy, 45(11): 6793–6805.

[19] Wang T., Yang C., Wang H., Ding S., and Daemen J. J. K. (2018). Debrining prediction of a salt cavern used for compressed air energy storage. Energy: 147: 464–476.

[20] Jaffré J. and Sboui A. (2010). Henry's law and gas phase disappearance. Transport in Porous Media, 82: 521–526.

[21] Grathwohl P. (1998). Diffusion in natural porous media: contaminant transport, sorption/desorption and dissolution kinetics. Springer US, New York.

[22] Pray A., Schweickert E. C., and Minnichi H. B. (1952). Solubility of Hydrogen, Oxygen, Nitrogen, and Helium in Water at elevated temperatures. Industrial and Engineering Chemistry, 44(5): 1146–1151.

[23] Diaz–Viera M. A., Lopez–Falcon D. A., Moctezuma–Berthier A., and Ortiz–Tapia A. (2008). COMSOL implementation of a multiphase flow model in porous media. *In* the Proceedings of the COMSOL conference, Boston, New York, USA.

[24] Beckermann C., Ramadhyani S., and Viskanta R. (1986). Natural convection flow and heat transfer between a fluid layer and a porous layer inside a rectangular enclosure. Journal of Heat Transfer, 109: 363–370.

[25] Bergholz R. F. (1978). Instability of steady natural convection in a vertical fluid layer. Journal of Fluid Mechanics, 2(84): 743–768.

[26] Kloppmann W., Négrel P. H., Casanova J., Klinge H., Schelkes K., and Guerrot C. (2001). Halite dissolution derived brines in the vicinity of a Permian salt dome (N German Basin). Evidence from boron, strontium, oxygen, and hydrogen isotopes. Geochimica et Cosmochimica Acta, 65(22): 4087–4101.

[27] Hassanizadeh S. M. and Leijnse T. (1988). On the Modeling of Brine Transport in Porous Media. Water Resources Research, 24(3): 321–330.

[28] Johnson K. S. (1981). Dissolution of salt on the east flank of the permian basin in the southwestern U.S.A. Journal of Hydrology, 54: 75–93.

[29] Gevantman L. H. (1981). Physical properties data for rock salt. U.S. Department of Commerce/National Bureau of Standards. U.S. Government Printing Office, Washington, D.C. 20402.

[30] Bradley J. S. (1975). Abnormal Formation Pressure. AAPG Bulletin, 59(6): 957–973.

[31] Ho C. K. and Webb S. W. (2006). Gas Transport in Porous Media. Springer, 3300 AA Dordrecht, The Netherlands.

[32] Wipf H. (2001). Solubility and Diffusion of Hydrogen in Pure Metals and Alloys. Physica Scripta, T94: 43–51.

[33] Hempelmann R. (1984). Diffusion of hydrogen in metals. Journal of the Less-Common Metals, 101: 69–96.

[34] Pfeiffer W. T., al Hagrey S. A., Köhn D., Rabbel W., and Bauer S. (2016). Porous media hydrogen storage at a synthetic, heterogeneous field site: numerical simulation of storage operation and geophysical monitoring. Environmental Earth Sciences, 75: 1177.

[35] Morel–Seytoux H. J., Meyer P. D., Nachabe M., Tourna J., van Genuchten M. T., and Lenhard R. J. (1996). Parameter equivalence for the Brooks–Corey and van Genuchten soil characteristics: preserving the effective capillary drive. Water Resources Research banner, 32(5): 1251–1258.

[36] AbuAisha M. and Rouabhi A. (2019). On the validity of the uniform thermodynamic state approach for underground caverns during fast and slow cycling. International Journal of Heat and Mass Transfer, 142: 118424.

[37] Rouabhi A., Hévin G., Soubeyran A., Labaune P., and Louvet F. (2017). A multiphase multi–component modeling approach of underground salt cavern storage. Geomechanics for Energy and the Environment, 12: 21–35.

[38] Angelini O., Chavant C., Chénier E., Eymard R., and Granet S. (2011). Finite volume approximation of a diffusion–dissolution model and application to nuclear waste storage. Mathematics and Computers in Simulation, 81(10): 2001–2017.

[39] Mahjoub M., Rouabhi A., Tijani M., Granet S., M'Jahad S., and Talandier J. (2018). Numerical study of Callovo-Oxfordian argillite expansion due to gas injection. International Journal of Geomechanics, 18(1): 04017134.

[40] Xu W. J., Shao H., Hesser J., Wang W., Schuster K., and Kolditz O. (2013). Coupled multiphase flow and elasto–plastic modelling of in–situ gas injection experiments in saturated claystone (Mont Terri Rock Laboratory). Engineering Geology, 157: 55–68.

[41] Côté J. and Konrad J. M. (2005). A generalized thermal conductivity model for soils and construction materials. Revue Canadienne de Géotechnique, 42(2): 443–458.

[42] van Genuchten M. T. (1980). A closed–form equation for predicting the hydraulic conductivity of unsaturated soils. Soil science society of America journal, 44(5): 892–898.

[43] Mualem Y. (1978). Hydraulic conductivity of unsaturated porous media: generalized macroscopic approach. Water Resources Research, 14(2): 325–334.

[44] Rebour V., Billiotte J., Deveughèle M., Jambon A., and Le Guen C. (1997). Molecular diffusion in water–saturated rocks: A new experimental method. Journal of contaminant hydrology, 28(1): 71–93.

[45] Cosenza Ph., Ghoreychi M., Bazargan–Sabet B., and de Marsily G. (1999). In situ rock salt permeability measurement for long term safety assessment of storage. International Journal of Rock Mechanics and Mining Sciences, 36: 509–526.

[46] Schulze O., Popp T., and Kern H. (2001). Development of damage and permeability in deforming rock salt. Engineering Geology, 61: 163–180.

[47] Bannach A., Wagler T., Walden S., and Klafki M. (2005). Technology enhancement for 1) inventory assessment and mechanical integrity testing of gas–filled solution mined caverns and 2) mechanical

integrity tests of solution mines and liquid storage caverns. GRI–05/0175 project final report, prepared for Gas Research Institute (contract number 8750), D–095596 Freiberg, Germany.

[48] Poppei J., Mayer G., Hubschwerlen N., and Resele G. (2006). Flooding of an abandoned salt mine modeling two–phase flow in complex mine structures. . *In* the Proceedings of the TOUGH Symposium, Lawrence Berkeley National Laboratory, Berkeley, California, May 15–17.

[49] Crozier T. E. and Yamamoto S. (1974). Solubility of hydrogen in water, seawater, and NaCl solutions. Journal of Chemical and Engineering Data, 19(3): 242–244.

[50] Lopez–Lazaro C., Bachaud P., Moretti I., and Ferrando N. (2019). Predicting the phase behavior of hydrogen in NaCl brines by molecular simulation for geological applications. BSGF – Earth Sciences Bulletin 190, 7.

[51] Senger R., Lanyon B., Marschall P., and Vomvoris S. (2008). Numerical modeling of the gas migration test at the Grimsel test site (Switzerland). Nuclear Technology, 164(2): 155–168.

[52] Ferrell T. R. and Himmelblau M. D. (1967). Diffusion Coefficients of Hydrogen and Helium in Water. AlChE Journal, 13(4): 702–708.

[53] Jockwer N. and Wieczorek K.(2008). ADDIGAS. Advective and diffusive gas transport in rock salt formations. GRS–234, contact number: 02 E 9824 project final report, Gesellschaft fuer Anlagen– und Reaktorsicherheit mbH (GRS), Berlin, Germany.

[54] Kunz O., and Wagner W. (2012). The GERG–2008 Wide–Range Equation of State for Natural Gases and Other Mixtures: An Expansion of GERG-2004. Journal of Physical and Chemical Reference Data, 57(11): 3032–3091.